mathematics

MDPI

Article

Mathematical Analysis of Unsteady Stagnation Point Flow of Radiative Casson Hybrid Nanofluid Flow over a Vertical Riga Sheet

Taqi A. M. Shatnawi [1], Nadeem Abbas [2] and Wasfi Shatanawi [2,3,*]

[1] Department of Mathematics, Faculty of Science, The Hashemite University, P.O. Box 330127, Zarqa 13133, Jordan
[2] Department of Mathematics and Sciences, College of Humanities and Sciences, Prince Sultan University, Riyadh 11586, Saudi Arabia
[3] Department of Medical Research, China Medical University Hospital, China Medical University, Taichung 40402, Taiwan
* Correspondence: wshatanawi@psu.edu.sa

Abstract: Heat and mass transfer study of hybrid nanomaterial Casson fluid with time-dependent flow over a vertical Riga sheet was deliberated under the stagnation region. In the presence of the Riga sheet in fluid flow models, this formulation was utilized to introduce Lorentz forces into the system. We considered the three models of hybrid nanomaterial fluid flow: namely, Yamada Ota, Tiwari Das, and Xue models. Two different nanoparticles, namely, SWCNT and MWCNT under base fluid (water) were studied. Under the flow suppositions, a mathematical model was settled using boundary layer approximations in terms of PDEs (partial differential equations). The system of PDEs (partial differential equations) was reduced into ODEs (ordinary differential equations) after applying suitable transformations. The reduced system, in terms of ODEs (ordinary differential equations), was solved by a numerical scheme, namely, the bvp4c method. The inspiration of the physical parameters is presented through graphs and tables. The curves of the velocity function deteriorated due to higher values of M. The Hartmann number is a ratio of electric force to viscous force. The electric forces increased due to higher values of the modified Hartmann number, ultimately declining the velocity function. The skin friction was reduced due to an incremental in ϖ, while the Nusselt number raised with higher values of ϖ. Physically, the Eckert number increased, which improved kinetic energy and, as a result, skin friction declined. The heat transfer rate increased as kinetic energy increased, and the Eckert number increased. The skin friction reduced due to physical enhancement of β_1, the shear thinning was enhanced which reduced the skin friction.

Keywords: hybrid Casson nanofluid; thermal slip; radiation effect; viscous dissipation; vertical Riga sheet

MSC: 58D30; 65C20; 30E25

Citation: Shatnawi, T.A.M.; Abbas, N.; Shatanawi, W. Mathematical Analysis of Unsteady Stagnation Point Flow of Radiative Casson Hybrid Nanofluid Flow over a Vertical Riga Sheet. *Mathematics* **2022**, *10*, 3573. https://doi.org/10.3390/math10193573

Academic Editor: Hovik Matevossian

Received: 8 August 2022
Accepted: 26 September 2022
Published: 30 September 2022

1. Introduction

The research of non-Newtonian liquids has received much interest because of the wide range of uses they have in engineering and industry, particularly in the extraction of crude oil from petroleum products, the development of syrup medications, and the creation of plastic materials. Hamid et al. [1] investigated the impacts of Casson nanofluid on a stretching surface. Hamid et al. [1] discussed the results of their stability analysis and dual solutions. Jamshed et al. [2] emphasized the influences of Casson nanofluid flow on stretching sheets under solar radiation. Recently, a few authors developed results about Casson fluid for diverse flow considerations, see Refs. [3–7].

The energy crisis is one of the most significant problems in the real world. Several investigators discussed several techniques to develop energy at less cost. In the past years, because common fluids such as water, ethylene glycol, and engine oil contain weaker heat transfer rates due to low thermal conductivity and because metals have higher thermal conductivity than conventional fluids, nanosized metals are added to

the ordinary fluids which enhanced the heat transfer rate due to the enhancement in thermal conductivity. For real-life problems, nanofluid is used in different procedures, namely, nano-technological and industrial processes such as nuclear reactors, cooling of electronic devices, vehicle cooling, vehicle thermal management, heat exchangers, and so on. Furthermore, magnetic nanofluids are effective in cancer therapy, wound treatment, artery blockage removal, magnetic resonance imaging, and a variety of other applications. Maleki et al. [8] debated the heat and mass transfer of nanofluid flow at the porous surface. Maleki et al. [9] highlighted the impacts of pseudoplastic nanofluid under heat generation and viscous dissipation on the permeable stretching sheet. Alazwari et al. [10] deliberated the inspiration of the non-Newtonian fluid flow of nanofluid on stretching sheets. Sajid et al. [11] highlighted the impacts of micropolar fluid flow on heated surfaces having chemical effects. Abu-Hamdeh et al. [12] studied the impact of thermal slip on the power law of nanofluid flow over a stretching surface. Aouinet et al. [13] analyzed the impacts of the turbulent boundary layer for nanofluid on a stretching plate. Recently, a few authors developed the results of nanofluid on an exponential stretching (see refs. [14–17]).

There is much interesting work on the comprehensive description of the nanofluid which is called hybrid nanofluid. A hybrid nanofluid is a mixture of two nanosized particles and base fluid water. In the early years, the experiments studied the effects of hybrid nanofluid. The researchers considered the two nanoparticles, namely, aluminum oxide and copper, with a water-based fluid and perceived the heat transfer rate. Another mixture of hybrid nanofluid is prepared by using the two nanoparticles single wall carbon nanotube and aluminum oxide with different base fluids, water and ethylene glycol. Hybrid nanofluid having the base fluid as ethylene glycol achieved much better heat transfer as compared to the hybrid nanofluid with the base fluid as water. Devi et al. [18] highlighted the effects of the hybrid nanofluid on a porous surface numerically. Heat and mass transfer of a hybrid nanofluid over a circular cylinder was discussed by Nadeem et al. [19]. They considered the MHD effects under the stagnation region. A few authors worked on the hybrid nanofluid for different flow assumptions and various physical aspects, see refs. [20–24].

The interest in magnetic hydrodynamics with hybrid nanofluid by developed by the authors due to several engineering applications and because they can be used to control the rate of heat transfer by using an external magnetic field. The Riga plate is an innovative magnetic device designed out of a cluster of changeless magnets and alternating electrodes arranged over a flat surface. In fluid flow models, this formulation is used to introduce Lorentz forces into the system. In many setups, especially in submarines, the setup is highly effective and advantageous for preventing boundary layer separations in fluid flow, which helps to reduce skin friction. Abbas et al. [23] discussed the impacts of micropolar fluid flow over the Riga surface. Recently, a few authors developed ideas about the Riga sheet under different fluid model considerations, see refs. [24–27].

We considered the incompressible time-dependent flow of Casson hybrid nanomaterial fluid flow over a vertical Riga sheet under the stagnation region. The influence of viscous dissipation, solid nanoparticle concentration, and nonlinear radiation implemented on the vertical Riga sheet was investigated. We considered the three models of hybrid nanomaterial fluid flow: namely, Yamada and Ota [28], Xue [29], and Tiwari and Das [30]. Two different nanoparticles, namely, SWCNT and MWCNT, under base fluid (water) were studied. Under the above suppositions, a mathematical model was constructed in differential equations (partial differential equations) utilizing BLA (boundary layer approximations). Under the flow suppositions, a mathematical model was settled using boundary layer approximations in terms of PDEs. The system of PDEs was reduced to ODEs after applying suitable transformations. The reduced system in terms of ODEs was solved by a numerical scheme, namely, the bvp4c method. The stagnation point flow of unsteady Casson hybrid nanofluid with nonlinear radiation over vertical Riga stretching sheet was not discussed using the three models of hybrid nanofluids: namely, Yamada and Ota [28], Xue [29], and Tiwari and Das [30] under the thermal slip. The impacts of involving physical parameters on the velocity profile, temperature profile, skin friction, and Nusselt number are presented

through graphs and tables. These results are newly and usefully discussed in the industrial and engineering fields.

2. Materials and Methods

The mathematical model of the time-dependent incompressible flow of Casson hybrid nanofluid $((SWCNT - MWCNT)/Water)$ on a vertical Riga stretching sheet, which is seen in Figure 1, was deliberated in this study. The stagnation point flow was considered in this analysis. In fluid flow models, this formulation was used to introduce Lorentz forces into the system. These Lorentz forces were produced by arranging magnets in a span-wise pattern with alternating electrodes parallel to the wall surface and fading exponentially as the distance from the plate rises. The stagnation point region ($a > 0$) was considered to analyze the influence of Casson hybrid nanofluid. Thermal slip condition was implemented on the vertical sheet. The transportation of mass and heat was explored in the aspects of viscous dissipation and nonlinear radiation impacts, respectively. Some mathematical expressions of the thermodynamics system are provided below.

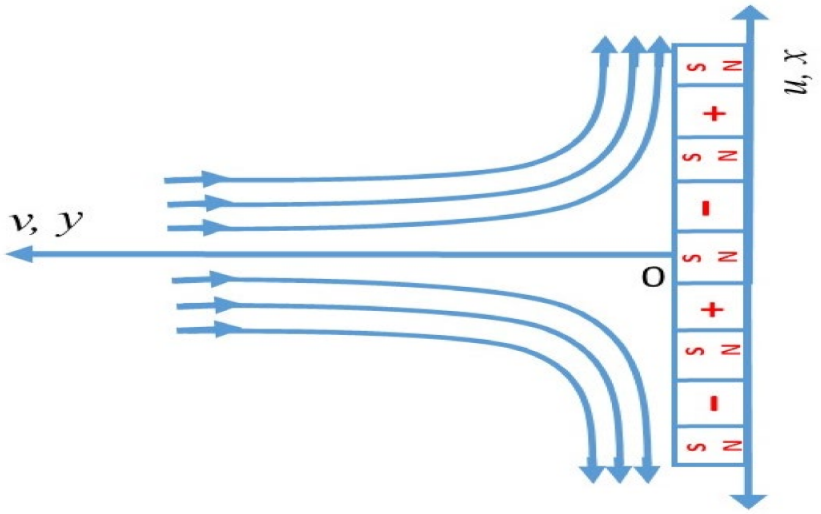

Figure 1. Flow pattern of Casson hybrid nanofluid over vertical Riga sheet.

Thermo-physical properties of hybrid nanofluid:

Effective properties of hybrid nanofluid are defined as below:

Density of hybrid nanofluid

The effective properties of SWCNT/water nanofluid and (SWCNT-MWCNT)/water hybrid nanofluid are defined as below:

$$\rho_{nf} = \phi_p \rho_p + (1 - \phi_p)\rho_{bf}. \tag{1}$$

Equation (1) is the introduced density of the nanofluid. The density of the hybrid nanofluid is defined as

$$\rho_{hnf} = \phi_{SWCNT}\rho_{SWCNT} + \phi_{MWCNT}\rho_{MWCNT} + (1 - \phi)\rho_{bf}. \tag{2}$$

ϕ is the total volume concentration of two different solid nanoparticle concentrations dispersed in hybrid nanofluid which is calculated as

$$\phi = \phi_{SWCNT} + \phi_{MWCNT}. \tag{3}$$

The specific heat capacity of the nanofluid is defined as

$$C_{nf} = \frac{\phi_p \rho_p C_p + (1 - \phi_p)\rho_{bf} C_{bf}}{\rho_{nf}}. \tag{4}$$

The heat capacity of the hybrid nanofluid is defined as

$$C_{hnf} = \frac{\phi_{SWCNT}\rho_{SWCNT}C_{SWCNT} + \phi_{MWCNT}\rho_{MWCNT}C_{MWCNT} + (1-\phi)\rho_{bf}C_{bf}}{\rho_{hnf}}. \quad (5)$$

The thermal expansion of the nanofluid is defined as

$$\beta_{nf} = \frac{\phi_p\rho_p\beta_p + (1-\phi_p)\rho_{bf}\beta_{bf}}{\rho_{nf}}. \quad (6)$$

The thermal expansion of the hybrid nanofluid is defined as

$$\beta_{hnf} = \frac{\phi_{SWCNT}\rho_{SWCNT}\beta_{SWCNT} + \phi_{MWCNT}\rho_{MWCNT}\beta_{MWCNT} + (1-\phi)\rho_{bf}\beta_{bf}}{\rho_{hnf}}. \quad (7)$$

The nanofluid models were proposed by Yamada and Ota [28] and Xue [29]. Tiwari and Das [30] proposed a hybrid nanofluid model. The Yamada and Ota [28] and Xue [29] models of nanofluid were extended by Abbas et al. [31] and Abbas et al. [32]. They considered the two solid nanoparticles in this analysis. The models of the hybrid nanofluid were introduced. The model of the hybrid nanofluid thermal conductivity was provided by Takabi and Salehi [33]. The expression of the Yamada-Ota model of hybrid nanofluid is presented below:

$$\frac{k_{hnf}}{k_{bf}} = \frac{\left\{\begin{array}{c} 1 + \frac{k_{bf}}{\frac{\phi_{SWCNT}k_{SWCNT}+\phi_{MWCNT}k_{MWCNT}}{\phi_{SWCNT}+\phi_{MWCNT}}}\frac{L}{R}(\phi_{SWCNT}+\phi_{MWCNT})^{0.2} \\ +\left(1 - \frac{k_{bf}}{\frac{\phi_{SWCNT}k_{SWCNT}+\phi_{MWCNT}k_{MWCNT}}{\phi_{SWCNT}+\phi_{MWCNT}}}\right)(\phi_{SWCNT}+\phi_{MWCNT})\frac{L}{R}(\phi_{SWCNT}+\phi_{MWCNT})^{0.2} \\ +2(\phi_{SWCNT}+\phi_{MWCNT})\left(\frac{\frac{\phi_{SWCNT}k_{SWCNT}+\phi_{MWCNT}k_{MWCNT}}{\phi_{SWCNT}+\phi_{MWCNT}}}{\frac{\phi_{SWCNT}k_{SWCNT}+\phi_{MWCNT}k_{MWCNT}}{\phi_{SWCNT}+\phi_{MWCNT}}-k_{bf}}\right)ln\left(\frac{\frac{\phi_{SWCNT}k_{SWCNT}+\phi_{MWCNT}k_{MWCNT}}{\phi_{SWCNT}+\phi_{MWCNT}}+k_{bf}}{2\frac{\phi_{SWCNT}k_{SWCNT}+\phi_{MWCNT}k_{MWCNT}}{\phi_{SWCNT}+\phi_{MWCNT}}}\right) \end{array}\right\}}{\left\{1-(\phi_{SWCNT}+\phi_{MWCNT}) + 2(\phi_{SWCNT}+\phi_{MWCNT})\left(\frac{k_{bf}}{\frac{\phi_{SWCNT}k_{SWCNT}+\phi_{MWCNT}k_{MWCNT}}{\phi_{SWCNT}+\phi_{MWCNT}}-k_{bf}}\right)ln\left(\frac{\frac{\phi_{SWCNT}k_{SWCNT}+\phi_{MWCNT}k_{MWCNT}}{\phi_{SWCNT}+\phi_{MWCNT}}+k_{bf}}{2k_{bf}}\right)\right\}}., \quad (8)$$

The expression of the Xue model of hybrid nanofluid are presented below:

$$\frac{k_{hnf}}{k_{bf}} = \frac{1-(\phi_{SWCNT}+\phi_{MWCNT}) + 2(\phi_{SWCNT}+\phi_{MWCNT})\left(\frac{\frac{\phi_{SWCNT}k_{SWCNT}+\phi_{MWCNT}k_{MWCNT}}{\phi_{SWCNT}+\phi_{MWCNT}}}{\frac{\phi_{SWCNT}k_{SWCNT}+\phi_{MWCNT}k_{MWCNT}}{\phi_{SWCNT}+\phi_{MWCNT}}-k_{bf}}\right)ln\left(\frac{\frac{\phi_{SWCNT}k_{SWCNT}+\phi_{MWCNT}k_{MWCNT}}{\phi_{SWCNT}+\phi_{MWCNT}}+k_{bf}}{2k_{bf}}\right)}{1-(\phi_{SWCNT}+\phi_{MWCNT}) + 2(\phi_{SWCNT}+\phi_{MWCNT})\left(\frac{k_{bf}}{\frac{\phi_{SWCNT}k_{SWCNT}+\phi_{MWCNT}k_{MWCNT}}{\phi_{SWCNT}+\phi_{MWCNT}}-k_{bf}}\right)ln\left(\frac{\frac{\phi_{SWCNT}k_{SWCNT}+\phi_{MWCNT}k_{MWCNT}}{\phi_{SWCNT}+\phi_{MWCNT}}+k_{bf}}{2k_{bf}}\right)}. \quad (9)$$

The expression of the Tiwari–Das model of the hybrid nanofluid is presented below (see ref. Takabi and Salehi [33]):

$$\frac{k_{hnf}}{k_{bf}} = \frac{\left\{\frac{\phi_{SWCNT}k_{SWCNT}+\phi_{MWCNT}k_{MWCNT}}{\phi_{SWCNT}+\phi_{MWCNT}} + 2k_{bf} + 2(\phi_{SWCNT}k_{SWCNT}+\phi_{MWCNT}k_{MWCNT}) - 2(\phi_{SWCNT}+\phi_{MWCNT})k_{bf}\right\}}{\left\{\frac{\phi_{SWCNT}k_{SWCNT}+\phi_{MWCNT}k_{MWCNT}}{\phi_{SWCNT}+\phi_{MWCNT}} + 2k_{bf} - (\phi_{SWCNT}k_{SWCNT}+\phi_{MWCNT}k_{MWCNT}) + (\phi_{SWCNT}+\phi_{MWCNT})k_{bf}\right\}}. \quad (10)$$

Table 1 shows the thermophysical propertoies of base fluid and solid nanoparticles. Tables 2 and 3 revealed the thermophysical characteristics of nanofluid and hybrid nanofluid for the three models of hybrid nanofluid: Yamada and Ota [28], Xue [29], and Tiwari and Das [30]. T_w is the wall temperature and T_∞ is the ambient temperature. The free stream velocity is $u_\infty = \frac{ax}{\sqrt{1-\alpha t}}$. The u and v are the velocity mechanisms along $-x$ and $-y$ directions, respectively. The fluid velocity and fluid temperature are u and T, respectively. The mathematical model is presented below.

Table 1. The physical properties of the solid nanoparticles and the base fluid.

Thermophysical Properties	MWCNT	SWCNT	H_2O
$\rho\left(\mathrm{Jkg^{-1}K^{-1}}\right)$	1600	2600	997.1
$k^*\left(\mathrm{kgm^{-3}}\right)$	3000	6600	0.613
$c_p\left(\mathrm{Wm^{-1}K^{-1}}\right)$	796	425	4179
$\beta/\mathrm{K^{-1}}$	1.6×10^{-6}	1.5×10^{-5}	21×10^{-5}

Table 2. Physical properties of hybrid nanofluid.

ϕ	ϕ_{SWCNT}	ϕ_{MWCNT}	ρ_{hnf}	$(C_p)_{hnf}$	k_{hnf} (Yamada-Ota Model)	k_{hnf} (Xue Model)	k_{hnf} (Tiwari-Das Model)
0.10	0.0038	0.0962	1061.19	3653.363	2.788343	2.711645	0.8172003
0.33	0.0125	0.3175	1194.612	2709.356	9.846296	9.510268	1.482817
0.75	0.0285	0.7215	1477.775	1348.05	59.00918	56.84039	6.117090
1.00	0.0380	0.9620	1638.000	773.6222	7311.015	7037.057	3136.800

Table 3. Physical properties of nanofluid.

ϕ	ρ_{nf}	$(C_p)_{nf}$	k_{nf} (Yamada-Ota Model)	k_{nf} (Xue Model)	k_{nf} (Tiwari-Das Model)
0.10	1157.39	3335.689	2.991149	2.914448	0.8172701
0.33	1526.057	2068.376	11.15951	10.80944	1.5184
0.75	2199.275	850.494	64.6763	62.49929	6.123857
1.00	2600.0	425.0	15169.65	14649.5	6600.0

$$\frac{\partial u}{\partial x} + \frac{\partial v}{\partial y} = 0, \tag{11}$$

$$\frac{\partial u}{\partial t} + u\frac{\partial u}{\partial x} + v\frac{\partial u}{\partial y} = \frac{\partial u_\infty}{\partial t} + u_\infty \frac{\partial u_\infty}{\partial x} + \nu_{hnf}\left(1 + \frac{1}{\beta_1}\right)\frac{\partial^2 u}{\partial y^2} + \frac{M_0\,\sigma^2}{8\,\pi\rho_{hnf}} e^{-\frac{\pi}{a}\,y} + \beta_{hnf} g(T - T_\infty), \tag{12}$$

$$\frac{\partial T}{\partial t} + u\frac{\partial T}{\partial x} + v\frac{\partial T}{\partial y} = \alpha_{hnf}\frac{\partial T}{\partial y^2} - \frac{1}{(\rho c)_{hnf}}\frac{\partial q_r}{\partial y} + \frac{\nu_{hnf}}{\left(\rho c_f\right)_{hnf}}\left(1 + \frac{1}{\beta_1}\right)\left(\frac{\partial u}{\partial y}\right)^2, \tag{13}$$

with respect to the boundary conditions being

$$\left.\begin{array}{c} v = 0, \quad u = 0, \quad T = T_w + \lambda_2 \frac{k_{hnf}}{k_f}\frac{\partial T}{\partial y}, \quad as\ y \to 0, \\ u = u_e, \quad T = T_\infty, \quad as\ y \to \infty. \end{array}\right\} \tag{14}$$

We introduced the suitable transformations as follows:

$$\left.\begin{array}{c} \eta = \sqrt{\frac{a}{v_f\ (1-\alpha t)}}y\ ,\ u = \frac{ax}{1-\alpha t}F'(\eta), \\ v = -\sqrt{\frac{a\ v_f}{1-\alpha t}}F(\eta)\ ,\ \theta(\eta) = \frac{T-T_\infty}{T_w - T_\infty}\ ,\ q_r = -\frac{16\ \sigma\ T^3}{3}\frac{\partial T}{\partial y}\ . \end{array}\right\}. \tag{15}$$

Applying the following transformation, the above equations are reduced as follows:

$$\left(\frac{1}{A_1} + \frac{1}{\beta_1}\right)\left(\frac{1}{B_1}\right)F'''(\eta) + 1 + \frac{Me^{-\tau\ \eta}}{B_1} + F(\eta)\ F''(\eta) - \left(F'(\eta)\right)^2 - \frac{\gamma_1}{B_1}\left(\frac{\eta}{2}F''(\eta) + F'(\eta) - 1\right) + 1 + B_2\delta\theta(\eta) = 0, \tag{16}$$

$$\left(\frac{1}{C_1}\right)\frac{k_{hnf}}{k_{bf}}\left(\frac{1}{\mathrm{Pr}}\right)\left(1+\frac{4}{3}\,R_d\right)\theta''(\eta)+\theta'(\eta)\,F(\eta)+\frac{\gamma_1}{2C_1}\,\eta\,\theta'(\eta)+\frac{\varpi}{C_1}\left(\frac{1}{A_1}+\frac{1}{\beta_1}\right)(F\prime\prime(\eta))^2. \tag{17}$$

With boundary conditions as follows:

$$F(0)=0,\quad F'(0)=0=\in,\quad F'(\infty)=1,\quad \theta(0)=1+\lambda\frac{k_{hnf}}{k_{bf}}\theta\prime(0),\quad \theta(\infty)=0. \tag{18}$$

where

$$A_1=((1-\phi_1)(1-\phi_2))^{2.5},\ B_1=(1-\phi_1)(1-\phi_2)+\phi_1\left(\frac{\rho_{s_1}}{\rho_f}\right)+\phi_2\left(\frac{\rho_{s_2}}{\rho_f}\right),\ C_1=\left((1-\phi_1)(1-\phi_2)+\phi_1\left(\frac{(\rho c_p)_{s_1}}{(\rho c_p)_f}\right)+\phi_2\left(\frac{(\rho c_p)_{s_2}}{(\rho c_p)_f}\right)\right),\ B_2=\frac{\beta_{hnf}}{\beta_{bf}}.$$

From an engineering perspective, the physical quantities such as skin friction and Nusselt number are the most significant. These quantities are defined as:

$$C_{fx}=\frac{\tau_x}{\rho_{hnf}{u_e}^2},\ \ Nu_x=\frac{xq_x}{k_f(T_w-T_\infty)}. \tag{19}$$

where τ_x and q_x are presented as

$$q_w=-k_{hnf}\left(1+\frac{4}{3}\,R_d\right)\left(\frac{\partial T}{\partial y}\right)\Big|_{y=0},\ \ \tau_x=\left(\mu_{hnf}+\frac{1}{\beta_1}\right)\left(\frac{\partial u}{\partial y}\right)\Big|_{y=0}. \tag{20}$$

In the dimensionless form

$$Nu_x(Re_x)^{-\frac{1}{2}}=-\frac{k_{hnf}}{k_{bf}}\left(1+\frac{4}{3}\,R_d\right)\theta''(\eta),\quad C_{fx}(Re_x)^{\frac{1}{2}}=\left(\frac{1}{A_1}+\frac{1}{\beta_1}\right)\left(\frac{1}{B_1}\right)F''(0). \tag{21}$$

The local Reynolds number is Re_x. The unsteadiness parameter is $\left(\gamma_1=\frac{\alpha}{a}\right)$, radiation parameter is $\left(R_d=\frac{16\,\sigma\,{T_\infty}^3}{3k_\infty k^*}\right)$, Prandtl number is $\left(Pr=\frac{\upsilon_f}{\alpha_f}\right)$, Casson fluid parameter is $\left(\beta_1=\frac{\mu_B\sqrt{2\pi_c}}{p_y}\right)$, Eckert number is $\left(\varpi=\frac{{U_w}^2}{c_p(T_w-T_\infty)}\right)$, buoyancy parameter is $\left(\delta=\frac{Gr_x}{{Re_x}^2}=\frac{gL_BT_B\beta_{bf}}{a^2}\right)$, modified Hartmann number is $\left(M=\frac{\pi M_0J_0}{8\rho_{bf}{U_w}^2}\right)$, and the magnetic dimensionless term is $\left(\tau=\frac{\pi}{a}{Re_x}^{-1}\right)$,

3. Numerical Procedure

The nonlinear ordinary differential equations were reduced into first-order differential equations which were solved through the bvp4c method by using Matlab packages. The description of the bvp4c methods is presented in Figure 2. The error of tolerance was 10^{-6}. The procedure is given below:

$$F(\eta)=s(1);\ \ F'(\eta)=s(2);\ \ F''(\eta)=s(3);\ F'''(\eta)=ss1; \tag{22}$$

$$ss1=-\left(\left(\frac{1}{A_1}+\frac{1}{\beta_1}\right)\frac{1}{B_1}\right)^{-1}\left(1+\frac{Me^{-\tau\,x}}{B_1}+y(1)y(3)-y(2)y(2)-\frac{\gamma_1}{B_1}\left(\frac{x}{2}y(3)+y(2)-1\right)+B_2\delta y(4)\right); \tag{23}$$

$$\theta(\eta)=s(4);\ \ \theta'(\eta)=s(5);\ \ \theta''(\eta)=ss2; \tag{24}$$

$$ss2 = -\left(\frac{1}{C_1}\right)^{-1} Pr\frac{k_{bf}}{k_{hnf}}\left(1+\frac{4}{3}R_d\right)^{-1}\left(s(5)s(1)+\frac{\gamma_1}{2}xs(5)+\frac{\varpi}{(C_1)}\left(\frac{1}{A_1}+\frac{1}{\beta_1}\right)s(3)s(3)\right). \quad (25)$$

With boundary conditions being

$$s0(1); s0(2); sinf(2)-1; s0(4)-1-\lambda\frac{k_{hnf}}{k_{bf}}s0(5); sinf(4); \quad (26)$$

The numerical results converged when the boundary residuals ($R_1(u_1, u_2)$, $R_2(u_1, u_2)$) were less than the tolerance error, i.e., 10^{-6}. When the numerical values became repeating, unless it ran into the compulsory convergence basis. The boundary residuals are as follows:

$$R_1(u_1\ u_2) = |y_2(\infty) - \hat{y_2}(\infty)|,$$

$$R_2(u_1\ u_2) = |y_4(\infty) - \hat{y_4}(\infty)|.$$

Hence, $\hat{y_2}(\infty)$ and $\hat{y_4}(\infty)$ were computed boundary values.

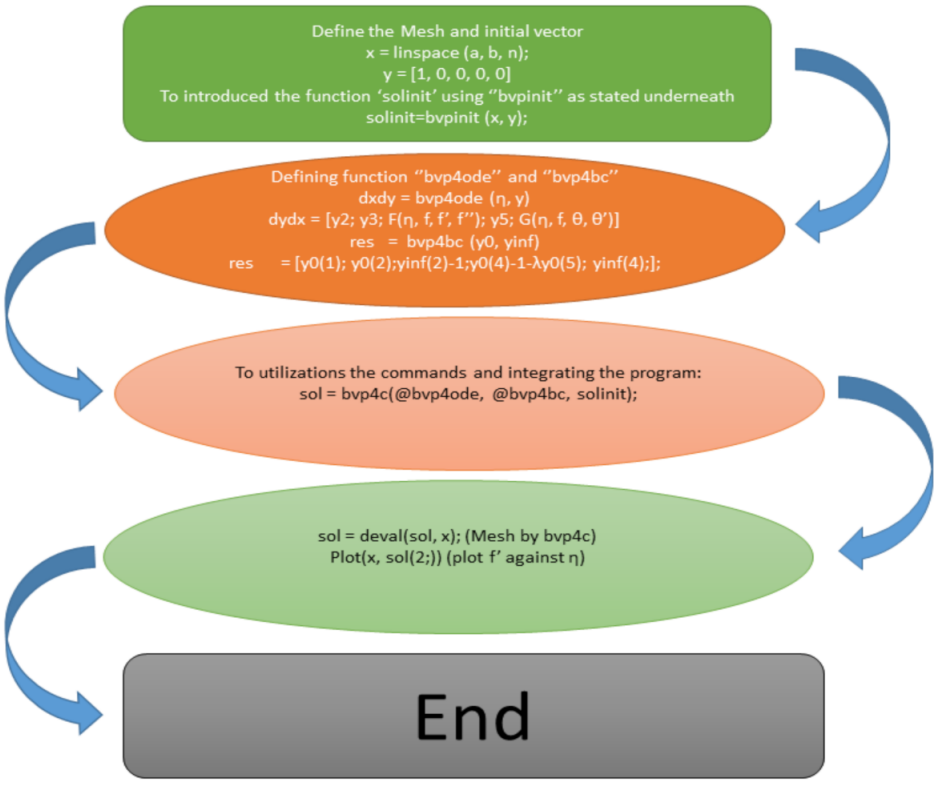

Figure 2. Disruption flow chat of numerical bv4c scheme.

4. Results and Discussion

The developed mathematical model of unsteady Casson hybrid nanofluid flow over a vertical Riga sheet was solved through numerical technique. The physical parameters being: Casson fluid parameter (β_1), modified Hartmann number (M), dimensionless parameter (τ), unsteadiness parameter (γ_1), buoyancy force (δ), radiation parameter (R_d), solid nanoparticle concentration (ϕ_2), Eckert number (ϖ), and thermal slip (λ) effects are presented through graphs and table. Figures 3–7 indicate the impacts of the Casson fluid parameter (β_1), solid nanoparticle concentration (ϕ_2), buoyancy force (δ), dimensionless parameter (τ), and modified Hartmann number (δ) on the velocity function. The influence of β_1 on the velocity function is presented in Figure 3. The curves of the velocity function

increased due to the incremental rise of β_1 because the viscosity of the fluid declined which boosted the fluid velocity at the surface of the vertical Riga sheet. The elasticity of the parameter was due to the relationship between relaxation and delay time. As the Casson parameter increased, the flow profile increased, indicating that the thickness of the lower confinement surface stopped at zero. In fact, the higher the Casson value, the higher the primary velocity for the Newton case. The impacts of ϕ_2 on the velocity function are revealed in Figure 4. The velocity function declined due to the incremental rise of ϕ_2 because the quantity of solid nanoparticles increased which increased the viscosity of the fluid which ultimately declines the fluid velocity. The higher values of ϕ_2, which mean increased resistance to the fluid motion, resulted in improved effective viscosity of the hybrid nanoparticles with base fluid which decreased the velocity of the fluid. Figure 5 indicates the impressions of M on the velocity function. The curves of the velocity function increased due to the higher values of M. The Hartmann number is a ratio of electric force to viscous force. The electric forces increased due to sophisticated values of M ultimately increasing the velocity function. The impacts of the buoyancy parameter (δ) on the velocity profile are presented in Figure 6. The curves of the velocity profile increased due to the augmentation of the buoyancy parameter (δ). It was noted that $\delta > 0$, $\delta < 0$, and $\delta = 0$ correspond to heated Riga sheet (assisting flow), cooled Riga sheet (opposing flow), and forced convection flow, respectively. We considered the heated Riga sheet (assisting flow) $\delta > 0$ in the present analysis. The fluid velocity increased due to the incremental rise in the buoyancy parameter (δ) because assisting flow raises the velocity of fluid. The variation of the unsteadiness parameter and velocity profile is presented in Figure 7. The velocity profile deteriorated due to the incremental rise of the unsteadiness parameter. In both profiles, this effect was accompanied by a decrease in the thickness of the momentum boundary layer, indicating that the unsteadiness parameter lowered the flowrate as a result of the stretching sheet.

Figures 8–13 indicate the impacts of the Casson fluid parameter (β_1), the solid nanoparticle concentration (ϕ_2), thermal slip (λ), the unsteadiness parameter (γ_1), the radiation parameter (R_d), and the Eckert number (ϖ) on the temperature function. The variation of β_1 and fluid temperature function is presented in Figure 8. The curves of fluid temperature function deteriorated due to higher values of β_1. Physically, the intention was that any rise in β_1 indicated a decline in the yield stress and, therefore, the thickness of the thermal boundary layer decreased. Figure 9 reveals the influence of ϕ_2 on the fluid temperature function. The curves of the fluid temperature function curves revealed an increasing trend due to the incremental rise of ϕ_2. The values of solid nanoparticle concentration (ϕ_2) increased which enhanced the curves of temperature function ($\theta(\eta)$). Physically, the thermal conductivity of the fluid was enhanced which enhanced the heat transfer rate. The variation of λ and fluid temperature function is presented in Figure 10. The curves of fluid temperature function deteriorated due to higher values of λ. Physically, the augmentation in thermal slip decreased the surface drag leading to a decay in the invention of heat quantity which deteriorated the temperature distribution. Figure 11 reveals the influence of γ_1 on the fluid temperature function. The curves of fluid temperature function curves revealed a decline due to the incremental rise of γ_1. We considered the heated Riga sheet (assisting flow). In this case, the steadiness parameter enhanced which decreased temperature of the surface. Figure 12 depicts the influence of R_d on fluid temperature function. The curves of fluid temperature increased due to the increasing values of R_d, but the behavior of the curves revealed the opposite at the point of infliction. As the values of the radiation parameter increased, the temperature of the fluid increased. As is known globally, the radiation increased, which enhanced the temperature of the surface. Figure 13 depicts the impacts of ϖ on the fluid temperature function. The curves of the temperature function increased due to the greater values of ϖ. The link between the kinetic energy in the flow and the enthalpy was expressed by the Eckert number. It was found that a rising Eckert number resulted in a rising temperature profile.

The influence of the Eckert number (ϖ), the solid nanoparticle concentration (ϕ_2), the Casson fluid parameter (β_1), the modified Hartmann number (M), the dimensionless parameter (τ), radiation parameter (R_d), and thermal slip (λ) on the skin friction ($C_{fx}(Re_x)^{\frac{1}{2}}$) and Nusselt number ($Nu_x(Re_x)^{-\frac{1}{2}}$) is depicted in Table 4. The influence of ϖ on the $C_{fx}(Re_x)^{\frac{1}{2}}$ and $Nu_x(Re_x)^{-\frac{1}{2}}$ is presented in Table 4. The skin friction reduced due to the incremental rise in ϖ while the Nusselt number rose with higher values of ϖ. The $Nu_x(Re_x)^{-\frac{1}{2}}$ improved due to incremental increases in the Eckert number (ϖ). The Eckert number implied that more thermal energy was added to the fluid so that heat was conducted from the plate into the fluid, i.e., causing an increase in heat transfer at the wall. The influence of ϕ_2 on $C_{fx}(Re_x)^{\frac{1}{2}}$ and $Nu_x(Re_x)^{-\frac{1}{2}}$ is presented in Table 4. The skin friction increased due to the higher values of ϕ_2. The heat transfer rate reduced due to the incremental rise in the values of ϕ_2. The influence of β_1 on the $C_{fx}(Re_x)^{\frac{1}{2}}$ and $Nu_x(Re_x)^{-\frac{1}{2}}$ is presented in Table 4. The skin friction reduced due to the physical enhancement of β_1; the shear thinning enhanced which reduced the skin friction. The Nusselt number declined due to the enhancement of β_1 because shear thinning enhanced which raised the heat transfer rate. Table 4 exposes the impressions of δ on the $C_{fx}(Re_x)^{\frac{1}{2}}$ and $Nu_x(Re_x)^{-\frac{1}{2}}$. It can be seen that both the $C_{fx}(Re_x)^{\frac{1}{2}}$ and $Nu_x(Re_x)^{-\frac{1}{2}}$ reduced due to the incremental increase in the δ. The variation of $C_{fx}(Re_x)^{\frac{1}{2}}$ and $Nu_x(Re_x)^{-\frac{1}{2}}$ with τ is presented in Table 4. The $C_{fx}(Re_x)^{\frac{1}{2}}$ enhanced but $Nu_x(Re_x)^{-\frac{1}{2}}$ decreased due to the higher values of τ. The variation of $C_{fx}(Re_x)^{\frac{1}{2}}$ and $Nu_x(Re_x)^{-\frac{1}{2}}$ with R_d is presented in Table 4. The $C_{fx}(Re_x)^{\frac{1}{2}}$ remained the same but $Nu_x(Re_x)^{-\frac{1}{2}}$ enhanced due to the higher values of R_d because thermal slip enhanced as well as the heat transfer increasing. As the radiation increased, which increased the heat transfer rate, ultimately, the temperature gradient increased. The variation of $C_{fx}(Re_x)^{\frac{1}{2}}$ and $Nu_x(Re_x)^{-\frac{1}{2}}$ with λ is presented in Table 4. The $C_{fx}(Re_x)^{\frac{1}{2}}$ remained the same but $Nu_x(Re_x)^{-\frac{1}{2}}$ enhanced due to the greater values of λ because thermal slip enhanced as well as the heat transfer increasing. Table 5 shows the comparative results of Wang [34] and Bachok et al. [35] with the present results. The present results were found to be similar with Wang's [34] and Bachok et al.'s [35] results. As the values of $\in$ increased and the skin friction declined. When $\in = 0$ means that the fluid and solid boundaries move at the same velocity, there is no friction at the fluid–solid interface.

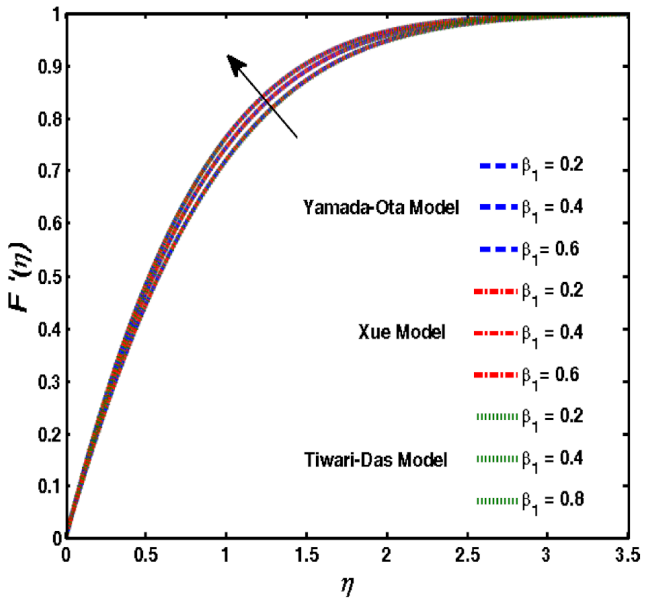

Figure 3. Influence of β_1 on $F'(\eta)$.

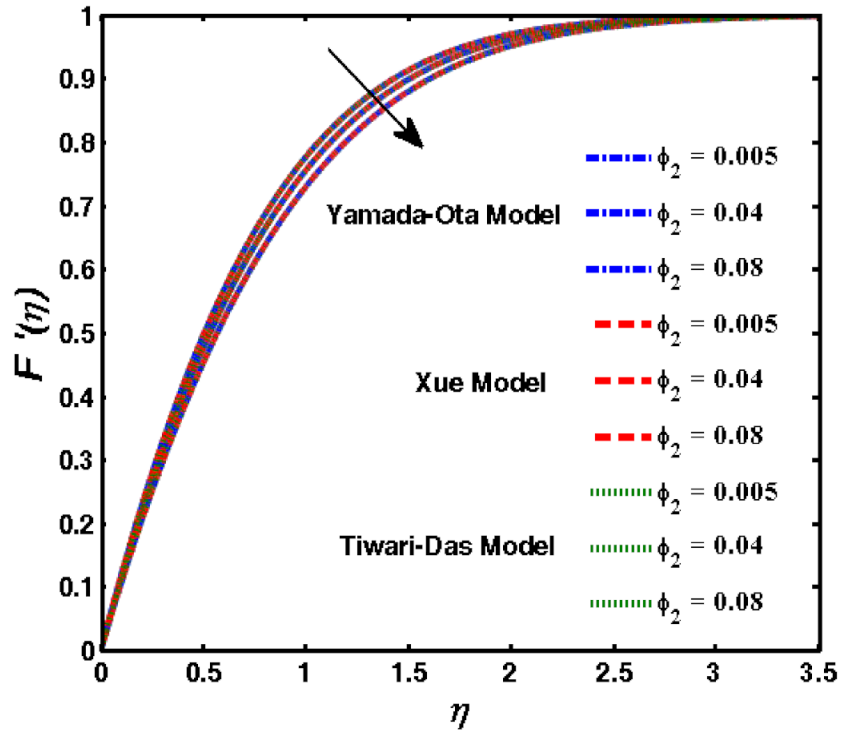

Figure 4. Influence of ϕ_2 on $F'(\eta)$.

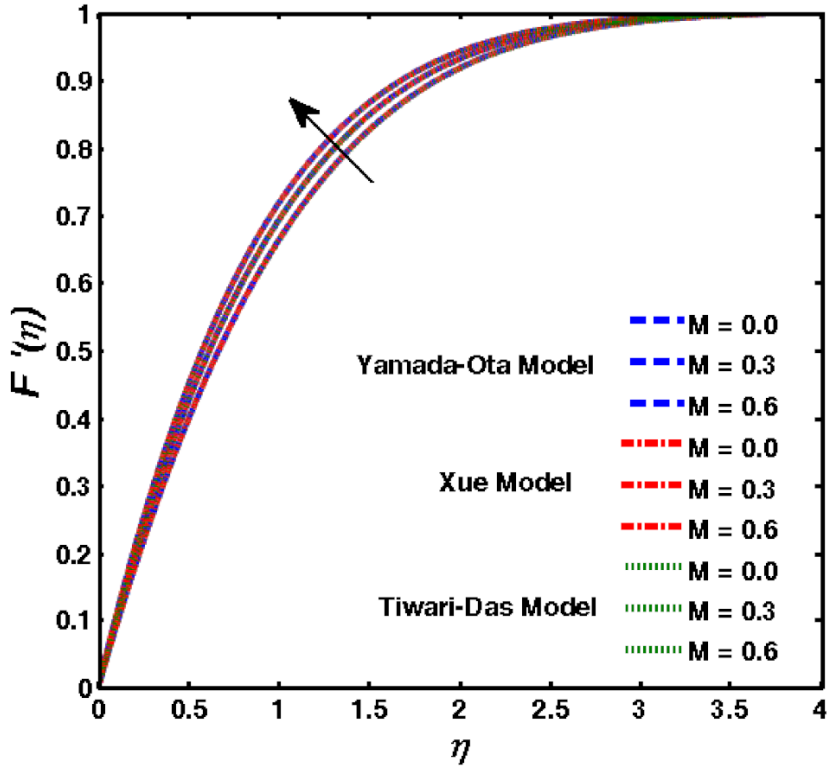

Figure 5. Influence of M on $F'(\eta)$.

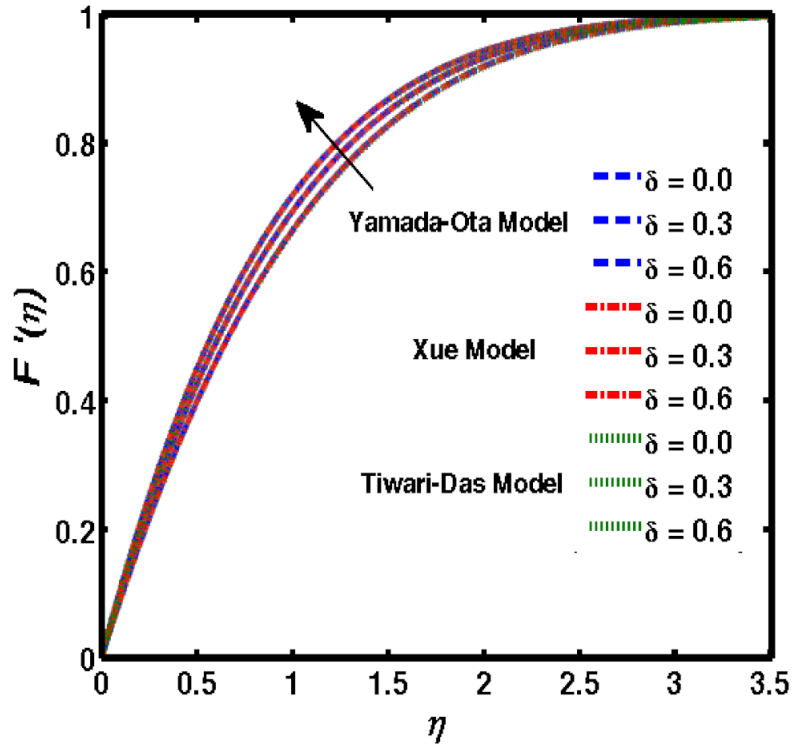

Figure 6. Influence of δ on $F'(\eta)$.

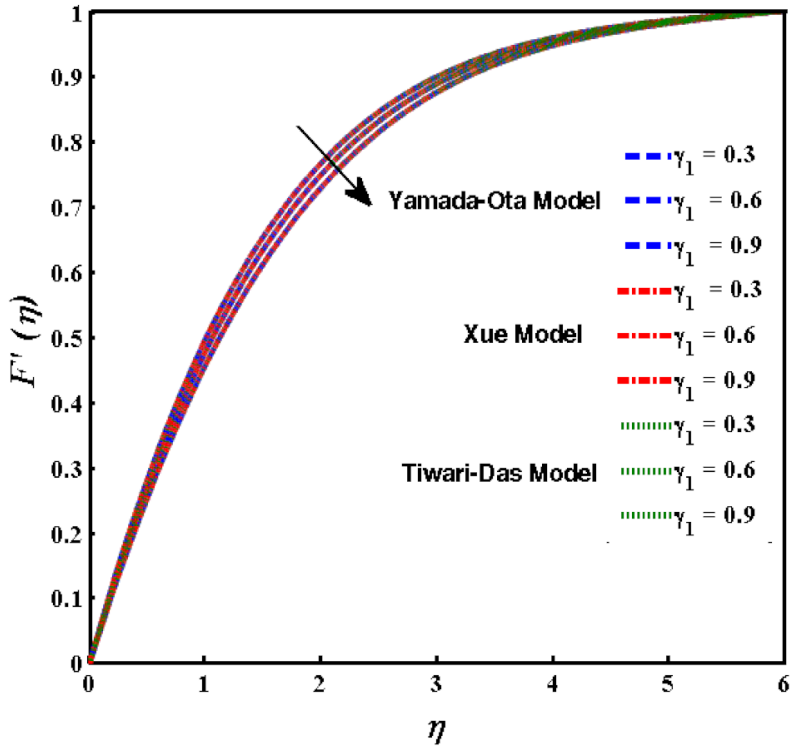

Figure 7. Influence of γ_1 on $F'(\eta)$.

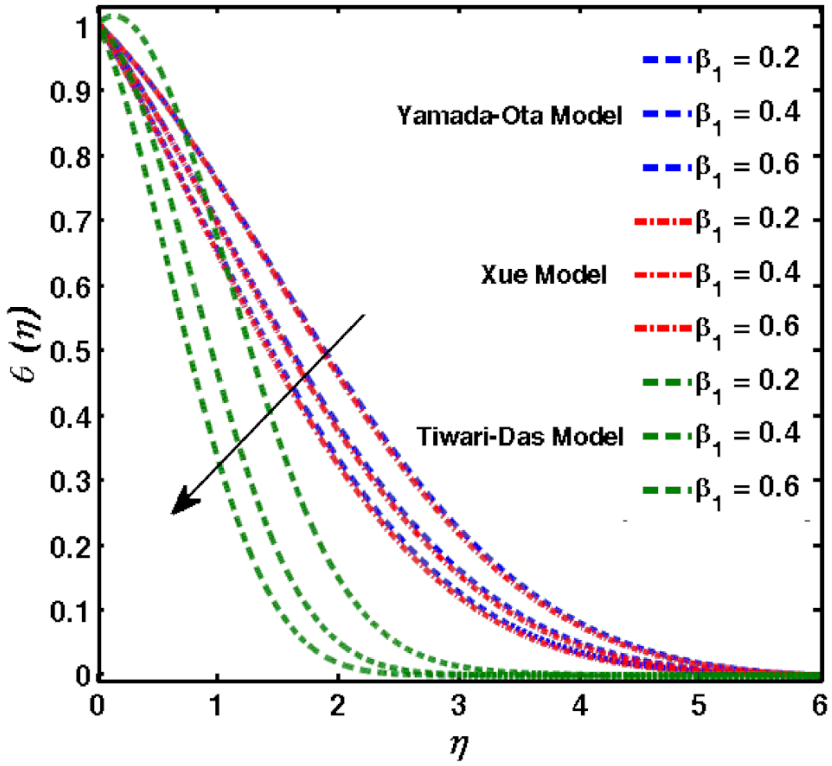

Figure 8. Influence of β_1 on $\theta(\eta)$ when $\lambda = 0.0$.

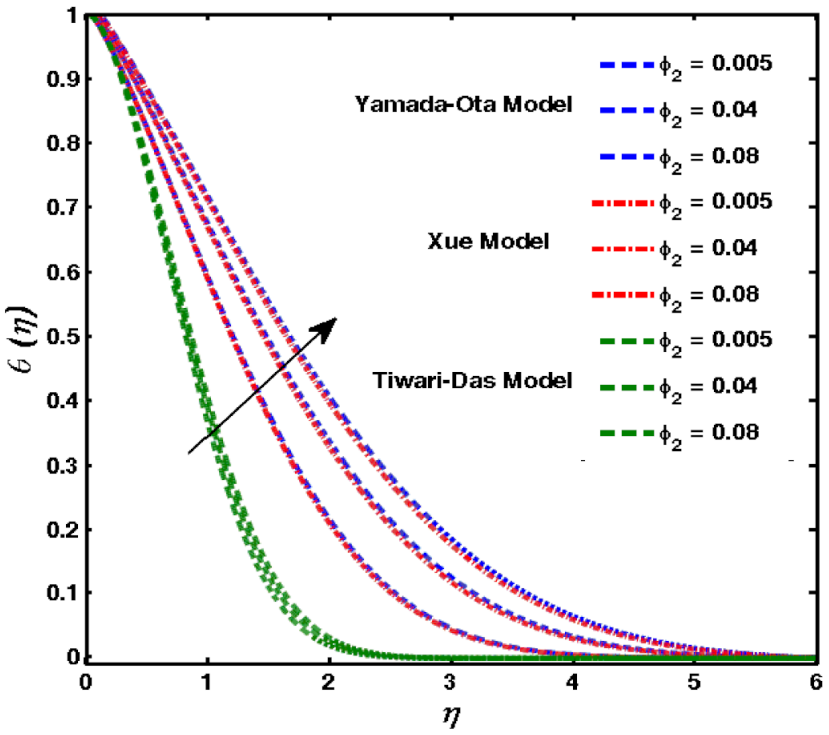

Figure 9. Influence of ϕ_2 on $\theta(\eta)$ when $\lambda = 0.0$.

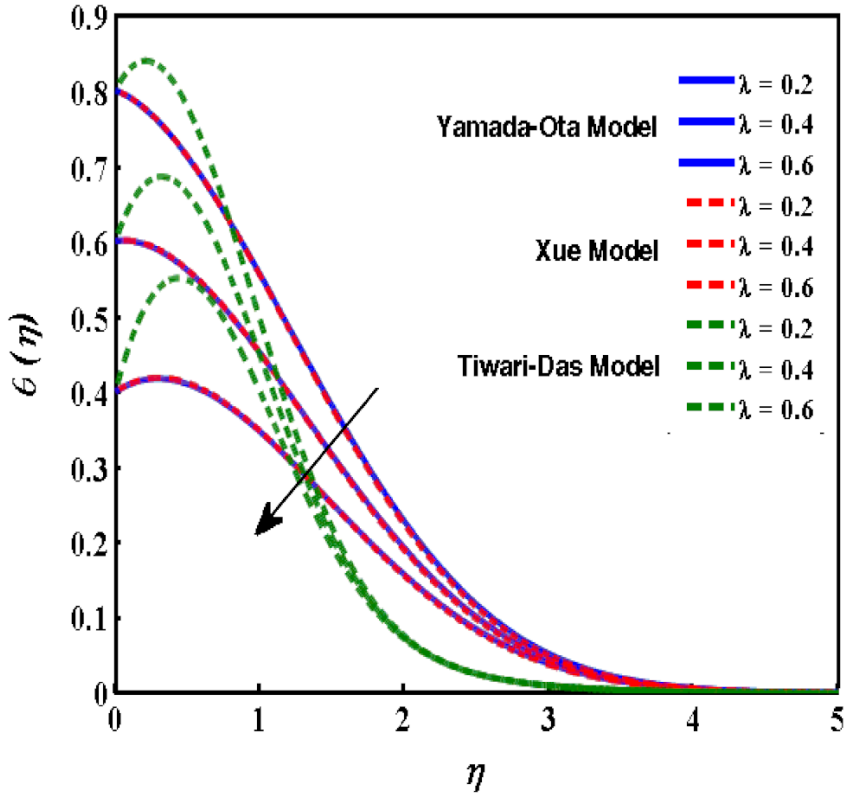

Figure 10. Influence of λ on $\theta(\eta)$.

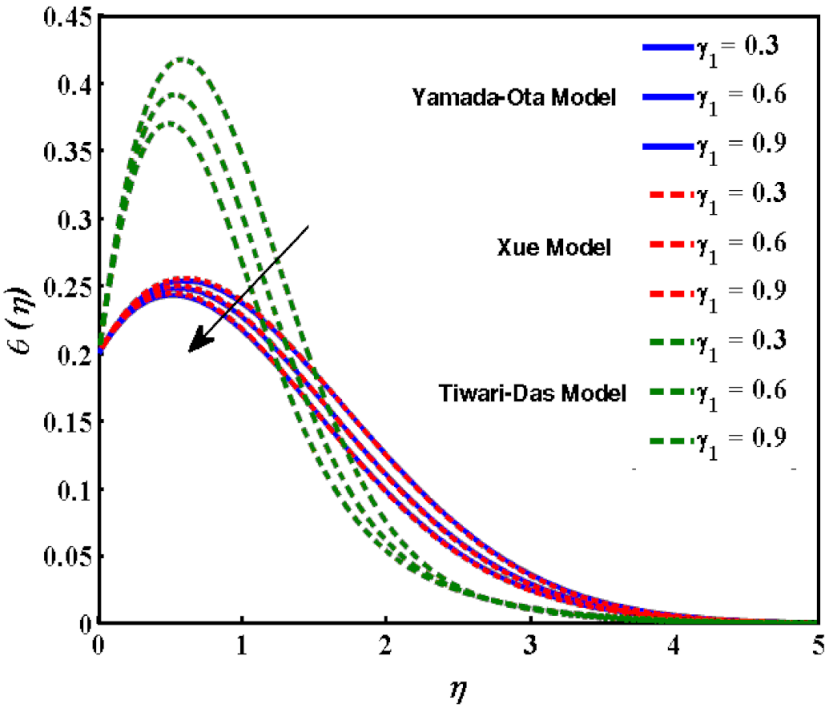

Figure 11. Influence of γ_1 on $\theta(\eta)$.

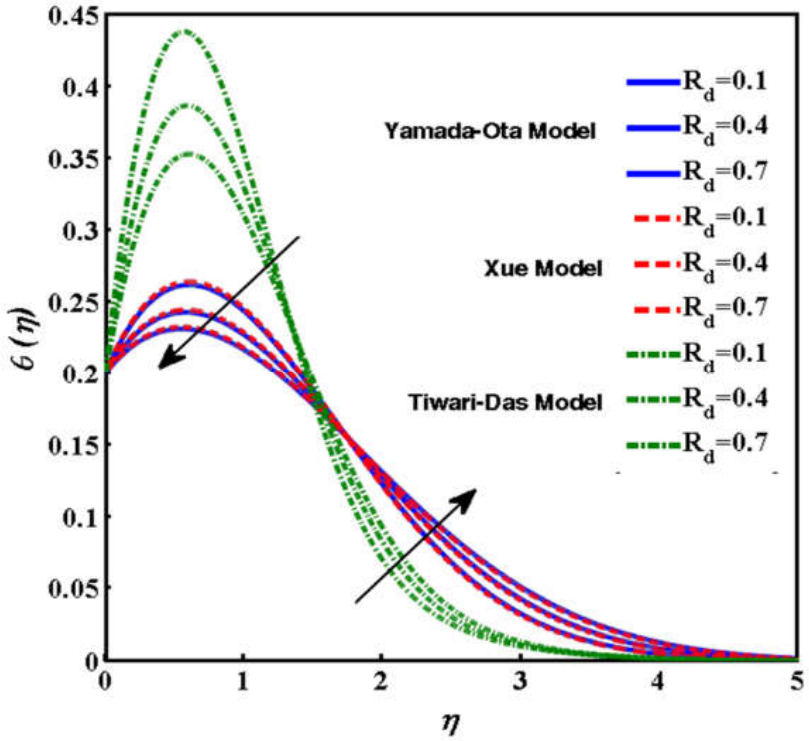

Figure 12. Influence of R_d on $\theta(\eta)$.

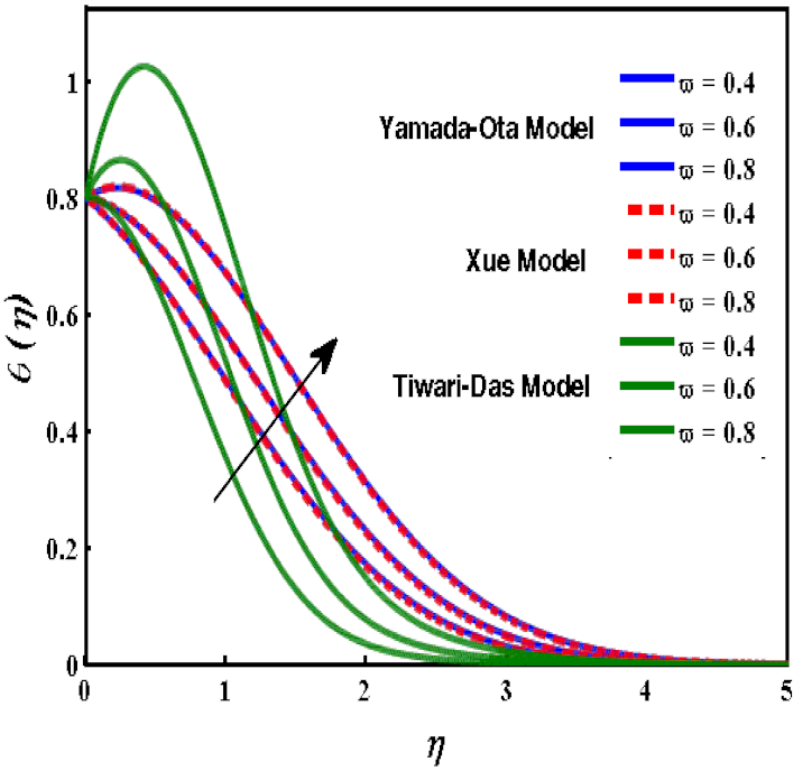

Figure 13. Influence of ω on $\theta(\eta)$.

Table 4. Numerical analysis of skin friction and Nusselt number for different values of parameters.

Physical Parameters							Yamada Ota Model		Xue Model		Tiwari Das Model	
ϖ	ϕ_2	β_1	M	τ	R_d	λ	$C_{fx}(Re_x)^{\frac{1}{2}}$	$Nu_x(Re_x)^{-\frac{1}{2}}$	$C_{fx}(Re_x)^{\frac{1}{2}}$	$Nu_x(Re_x)^{-\frac{1}{2}}$	$C_{fx}(Re_x)^{\frac{1}{2}}$	$Nu_x(Re_x)^{-\frac{1}{2}}$
0.1	0.04	0.3	0.4	0.5	0.3	0.2	2.5583	0.0188	2.5583	0.0188	2.5583	0.3323
0.2	-	-	-	-	-	-	2.5307	0.0195	2.5307	0.0195	2.5307	0.3586
0.3	-	-	-	-	-	-	2.5039	0.0201	2.5039	0.0201	2.5039	0.3843
0.4	-	-	-	-	-	-	2.4778	0.0208	2.4778	0.0208	2.4778	0.4094
0.1	0.02	-	-	-	-	-	2.2483	0.0428	2.2559	0.0295	2.2483	0.3890
-	0.04	-	-	-	-	-	2.4000	0.0269	2.4075	0.0210	2.4000	0.3594
-	0.06	-	-	-	-	-	2.5583	0.0188	2.5653	0.0159	2.5583	0.3323
-	0.08	-	-	-	-	-	2.7237	0.0140	2.7300	0.0125	2.7237	0.3073
-	0.04	0.1	-	-	-	-	3.9474	0.0349	3.9069	0.0135	3.9474	0.2681
-	-	0.3	-	-	-	-	2.4843	0.0414	2.4075	0.0210	2.4843	0.3670
-	-	0.5	-	-	-	-	2.0950	0.0438	2.0165	0.0237	2.0950	0.4045
-	-	0.7	-	-	-	-	1.9057	0.0451	1.8283	0.0250	1.9057	0.4251
-	-	0.3	0.2	-	-	-	3.7956	0.0265	2.5902	0.0287	2.5902	0.2625
-	-	-	0.4	-	-	-	3.4900	0.0082	2.4075	0.0210	2.4075	−0.046
-	-	-	0.6	-	-	-	3.1814	−0.012	2.2231	0.0126	2.2231	−0.383
-	-	-	0.8	-	-	-	2.8697	−0.035	2.0370	0.0033	2.0370	−0.753
-	-	-	0.4	0.1	-	-	3.7358	0.0541	3.7458	0.0272	3.7458	0.0541
-	-	-	-	0.3	-	-	3.7458	0.0261	3.8344	0.0279	3.8344	0.0652
-	-	-	-	0.5	-	-	3.8344	0.0267	3.8902	0.0283	3.8902	0.0717
-	-	-	-	0.7	-	-	3.8902	0.0271	3.9276	0.0286	3.9276	0.0758
-	-	-	-	0.5	0.0	-	3.9276	0.0144	3.9276	0.0254	3.9276	0.0488
-	-	-	-	-	0.3	-	3.9276	0.0244	3.9276	0.0346	3.9276	0.1280
-	-	-	-	-	0.6	-	3.9276	0.0331	3.9276	0.0430	3.9276	0.2025
-	-	-	-	-	0.9	-	3.9276	0.0411	3.9276	0.0509	3.9276	0.2731
-	-	-	-	-	0.3	0.0	3.9276	0.0648	3.9276	0.0680	3.9276	0.0680
-	-	-	-	-	-	0.2	3.9276	0.0486	3.9276	0.0509	3.9276	0.0509
-	-	-	-	-	-	0.4	3.9276	0.0324	3.9276	0.0338	3.9276	0.0338
-	-	-	-	-	-	0.6	3.9276	0.0162	3.9276	0.0167	3.9276	0.0167

Table 5. Comparative results of Wang [34] and Bachok et al. [35] with existent outcomes when the rest of the physical parameters are zero.

$\in$.	Wang [34]	Bachok et al. [35]	Present Results
0.0	1.232588	1.232588	1.229874
0.5	0.71330	0.713295	0.711874
1.0	0.0	0.0	0.0

5. Conclusions

The incompressible time-dependent flow of Casson hybrid nanomaterial fluid flow over a vertical Riga sheet under the stagnation region was considered. The three models of hybrid nanomaterial fluid flow: namely, Yamada–Ota, Tiwari–Das, and Xue models were discussed. Two different nanoparticles, namely, SWCNT and MWCNT under base fluid (water) were studied. The dimensionless system ODEs were solved by numerical scheme. The main achievements were as follows:

- The velocity function revealed a decline due to the incremental rise of ϕ_2 because the quantity of solid nanoparticle increased which increased the viscosity of the fluid which, ultimately, decreases the fluid velocity.
- The curves of velocity function declined due to the higher values of M. The Hartmann number is the ratio of electric force to viscous force. The electric forces increased due to the higher values of the modified Hartmann number, which, ultimately, decreased the velocity function.

- The skin friction reduced due to the enhancement of β_1; physically, the shear thinning enhanced which reduced the skin friction. The Nusselt number decreased due to the enhancement of β_1 because the shear thinning enhanced which raised the heat transfer rate.
- The $C_{fx}(Re_x)^{\frac{1}{2}}$ remained the same but $Nu_x(Re_x)^{-\frac{1}{2}}$ enhanced due to the higher values of R_d because the thermal slip enhanced as well as the heat transfer increasing. As the radiation increased, which, ultimately, increased the heat transfer rate, the temperature gradient increased because of the greater radiative structures characteristic of higher Nusselt numbers.

Author Contributions: Methodology, T.A.M.S.; Supervision, W.S.; Writing—original draft, N.A. All authors have read and agreed to the published version of the manuscript.

Funding: The authors (Nadeem Abbas and Wasfi Shatanawi) would like to acknowledge the support of Prince Sultan University for paying the article publication fee of this publication.

Data Availability Statement: Not applicable.

Acknowledgments: Nadeem Abbas and Wasfi Shatanawi wish to express their gratitude to Prince Sultan University for facilitating the publication of this article through the research lab Theoretical and Applied Sciences Lab (TAS).

Conflicts of Interest: The authors declare no conflict of interest.

References

1. Hamid, M.; Usman, M.; Khan, Z.H.; Ahmad, R.; Wang, W. Dual solutions and stability analysis of flow and heat transfer of Casson fluid over a stretching sheet. *Phys. Lett. A* **2019**, *383*, 2400–2408. [CrossRef]
2. Jamshed, W.; Goodarzi, M.; Prakash, M.; Nisar, K.S.; Zakarya, M.; Abdel-Aty, A.H. Evaluating the unsteady Casson nanofluid over a stretching sheet with solar thermal radiation: An optimal case study. *Case Stud. Therm. Eng.* **2021**, *26*, 101160. [CrossRef]
3. Maleki, H.; Safaei, M.R.; Alrashed, A.A.; Kasaeian, A. Flow and heat transfer in non-Newtonian nanofluids over porous surfaces. *J. Therm. Anal. Calorim.* **2019**, *135*, 1655–1666. [CrossRef]
4. Amjad, M.; Zehra, I.; Nadeem, S.; Abbas, N.; Saleem, A.; Issakhov, A. Influence of Lorentz force and induced magnetic field effects on Casson micropolar nanofluid flow over a permeable curved stretching/shrinking surface under the stagnation region. *Surf. Interfaces* **2020**, *21*, 100766. [CrossRef]
5. Kasim, A.R.M.; Arifin, N.S.; Ariffin, N.A.N.; Salleh, M.Z.; Anwar, M.I. Mathematical model of simultaneous flow between Casson fluid and dust particle over a vertical stretching sheet. *Int. J. Integr. Eng.* **2020**, *12*, 253–260.
6. Zehra, I.; Abbas, N.; Amjad, M.; Nadeem, S.; Saleem, S.; Issakhov, A. Casson nanoliquid flow with Cattaneo-Christov flux analysis over a curved stretching/shrinking channel. *Case Stud. Therm. Eng.* **2021**, *27*, 101146. [CrossRef]
7. Khan, M.N.; Nadeem, S. A comparative study between linear and exponential stretching sheet with double stratification of a rotating Maxwell nanofluid flow. *Surf. Interfaces* **2021**, *22*, 100886. [CrossRef]
8. Maleki, H.; Alsarraf, J.; Moghanizadeh, A.; Hajabdollahi, H.; Safaei, M.R. Heat transfer and nanofluid flow over a porous plate with radiation and slip boundary conditions. *J. Cent. South Univ.* **2019**, *26*, 1099–1115. [CrossRef]
9. Maleki, H.; Safaei, M.R.; Togun, H.; Dahari, M. Heat transfer and fluid flow of pseudo-plastic nanofluid over a moving permeable plate with viscous dissipation and heat absorption/generation. *J. Therm. Anal. Calorim.* **2019**, *135*, 1643–1654. [CrossRef]
10. Alazwari, M.A.; Abu-Hamdeh, N.H.; Goodarzi, M. Entropy optimization of first-grade viscoelastic nanofluid flow over a stretching sheet by using classical Keller-box scheme. *Mathematics* **2021**, *9*, 2563. [CrossRef]
11. Sajid, T.; Jamshed, W.; Shahzad, F.; Eid, M.R.; Alshehri, H.M.; Goodarzi, M.; Nisar, K.S. Micropolar fluid past a convectively heated surface embedded with nth order chemical reaction and heat source/sink. *Phys. Scr.* **2021**, *96*, 104010. [CrossRef]
12. Abu-Hamdeh, N.H.; Alsulami, R.A.; Rawa, M.J.; Alazwari, M.A.; Goodarzi, M.; Safaei, M.R. A Significant Solar Energy Note on Powell-Eyring Nanofluid with Thermal Jump Conditions: Implementing Cattaneo-Christov Heat Flux Model. *Mathematics* **2021**, *9*, 2669. [CrossRef]
13. Aouinet, H.; Dhahri, M.; Safaei, M.R.; Sammouda, H.; Anqi, A.E. Turbulent boundary layers and hydrodynamic flow analysis of nanofluids over a plate. *J. Cent. South Univ.* **2021**, *28*, 3340–3353. [CrossRef]
14. Waqas, H.; Farooq, U.; Alshehri, H.M.; Goodarzi, M. Marangoni-bioconvectional flow of Reiner–Philippoff nanofluid with melting phenomenon and nonuniform heat source/sink in the presence of a swimming microorganisms. *Math. Methods Appl. Sci.* **2021**, *in press*. [CrossRef]
15. Waqas, H.; Farooq, U.; Khan, S.A.; Alshehri, H.M.; Goodarzi, M. Numerical analysis of dual variable of conductivity in bioconvection flow of Carreau–Yasuda nanofluid containing gyrotactic motile microorganisms over a porous medium. *J. Therm. Anal. Calorim.* **2021**, *145*, 2033–2044. [CrossRef]

16. Imran, M.; Farooq, U.; Waqas, H.; Anqi, A.E.; Safaei, M.R. Numerical performance of thermal conductivity in Bioconvection flow of cross nanofluid containing swimming microorganisms over a cylinder with melting phenomenon. *Case Stud. Therm. Eng.* **2021**, *26*, 101181. [CrossRef]
17. Wang, F.; Ahmad, S.; Al Mdallal, Q.; Alammari, M.; Khan, M.N.; Rehman, A. Natural bio-convective flow of Maxwell nanofluid over an exponentially stretching surface with slip effect and convective boundary condition. *Sci. Rep.* **2022**, *12*, 2220. [CrossRef]
18. Devi, S.A.; Devi, S.S.U. Numerical investigation of hydromagnetic hybrid Cu–Al_2O_3/water nanofluid flow over a permeable stretching sheet with suction. *Int. J. Nonlinear Sci. Numer. Simul.* **2016**, *17*, 249–257. [CrossRef]
19. Nadeem, S.; Abbas, N.; Khan, A.U. Characteristics of three dimensional stagnation point flow of Hybrid nanofluid past a circular cylinder. *Results Phys.* **2018**, *8*, 829–835. [CrossRef]
20. Al-Hanaya, A.M.; Sajid, F.; Abbas, N.; Nadeem, S. Effect of SWCNT and MWCNT on the flow of micropolar hybrid nanofluid over a curved stretching surface with induced magnetic field. *Sci. Rep.* **2020**, *10*, 8488. [CrossRef]
21. Abbas, N.; Nadeem, S.; Saleem, A.; Malik, M.Y.; Issakhov, A.; Alharbi, F.M. Models base study of inclined MHD of hybrid nanofluid flow over nonlinear stretching cylinder. *Chin. J. Phys.* **2021**, *69*, 109–117. [CrossRef]
22. Li, P.; Duraihem, F.Z.; Awan, A.U.; Al-Zubaidi, A.; Abbas, N.; Ahmad, D. Heat Transfer of Hybrid Nanomaterials Base Maxwell Micropolar Fluid Flow over an Exponentially Stretching Surface. *Nanomaterials* **2022**, *12*, 1207. [CrossRef]
23. Abbas, N.; Nadeem, S.; Malik, M.Y. Theoretical study of micropolar hybrid nanofluid over Riga channel with slip conditions. *Phys. A Stat. Mech. Appl.* **2020**, *551*, 124083. [CrossRef]
24. Nadeem, S.; Malik, M.Y.; Abbas, N. Heat transfer of three-dimensional micropolar fluid on a Riga plate. *Can. J. Phys.* **2020**, *98*, 32–38. [CrossRef]
25. Nadeem, S.; Amin, A.; Abbas, N.; Saleem, A.; Alharbi, F.M.; Hussain, A.; Issakhov, A. Effects of heat and mass transfer on stagnation point flow of micropolar Maxwell fluid over Riga plate. *Sci. Iran.* **2021**, *28*, 3753–3766.
26. Prasad, K.V.; Vaidya, H.; Mebarek-Oudina, F.; Choudhari, R.; Nisar, K.S.; Jamshed, W. Impact of surface temperature and convective boundary conditions on a Nanofluid flow over a radially stretched Riga plate. *Proc. Inst. Mech. Eng. Part E J. Process Mech. Eng.* **2022**, *236*, 942–952. [CrossRef]
27. Tabassum, R.; Al-Zubaidi, A.; Rana, S.; Mehmood, R.; Saleem, S. Slanting transport of hybrid (MWCNTs-SWCNTs/H_2O) nanofluid upon a Riga plate with temperature dependent viscosity and thermal jump condition. *Int. Commun. Heat Mass Transf.* **2022**, *135*, 106165. [CrossRef]
28. Yamada, E.; Ota, T. Effective thermal conductivity of dispersed materials. *Wärme Stoffübertrag.* **1980**, *13*, 27–37. [CrossRef]
29. Xue, Q.Z. Model for thermal conductivity of carbon nanotube-based composites. *Phys. B* **2005**, *368*, 302–307. [CrossRef]
30. Tiwari, R.K.; Das, M.K. Heat transfer augmentation in a two-sided lid-driven differentially heated square cavity utilizing nanofluids. *Int. J. Heat Mass Transf.* **2007**, *50*, 2002–2018. [CrossRef]
31. Abbas, N.; Nadeem, S.; Malik, M.Y. On extended version of Yamada–Ota and Xue models in micropolar fluid flow under the region of stagnation point. *Phys. A Stat. Mech. Its Appl.* **2020**, *542*, 123512. [CrossRef]
32. Abbas, N.; Malik, M.Y.; Nadeem, S.; Alarifi, I.M. On extended version of Yamada–Ota and Xue models of hybrid nanofluid on moving needle. *Eur. Phys. J. Plus* **2020**, *135*, 1–16. [CrossRef]
33. Takabi, B.; Salehi, S. Augmentation of the heat transfer performance of a sinusoidal corrugated enclosure by employing hybrid nanofluid. *Adv. Mech. Eng.* **2014**, *6*, 147059. [CrossRef]
34. Wang, C.Y. Stagnation flow towards a shrinking sheet. *Int. J. Non-Linear Mech.* **2008**, *43*, 377–382. [CrossRef]
35. Bachok, N.; Ishak, A.; Pop, I. Stagnation-point flow over a stretching/shrinking sheet in a nanofluid. *Nanoscale Res. Lett.* **2011**, *6*, 623. [CrossRef]